

Massive MIMO with 1-bit ADC

Chiara Risi, Daniel Persson, and Erik G. Larsson

Abstract—We investigate massive multiple-input-multiple-output (MIMO) uplink systems with 1-bit analog-to-digital converters (ADCs) on each receiver antenna. Receivers that rely on 1-bit ADC do not need energy-consuming interfaces such as automatic gain control (AGC). This decreases both ADC building and operational costs. Our design is based on maximal ratio combining (MRC), zero-forcing (ZF), and least squares (LS) detection, taking into account the effects of the 1-bit ADC on channel estimation.

Through numerical results, we show good performance of the system in terms of mutual information and symbol error rate (SER). Furthermore, we provide an analytical approach to calculate the mutual information and SER of the MRC receiver. The analytical approach reduces complexity in the sense that a symbol and channel noise vectors Monte Carlo simulation is avoided.

Index Terms—Massive MIMO, large-scale antenna systems, analog-to-digital converter, 1-bit ADC.

I. INTRODUCTION

MIMO systems have attracted significant research interest during the last decade, and are incorporated into emerging wireless broadband standards like Long-Term Evolution (LTE) [1]. In order to perform the receive processing, the received analog baseband signal is converted into digital form using a couple of analog-to-digital converters per antenna, i.e., one sampler each for the in-phase and quadrature components.

There are several types of ADC. One ADC type is the flash. It consists of 2^b comparators, where b is the ADC resolution in bits. The receive voltage is divided over a resistive ladder with comparators measuring over different parts of the ladder. The comparators whose thresholds are less than their fed voltage give a non-zero output signal. These measurements are then transformed to bits. An important part of the flash ADC is the automatic gain control, which amplifies the received signal so as to match it to the range of the resistor ladder and comparators. Other ADC architectures are pipelined ADC and sigma-delta ADC [2].

Irrespectively of ADC technology, more output bits requires more operational power. There are several MIMO studies that take into account the effects of the ADC on the performance evaluation of the system. The paper [3] examines the ADC effects with a ZF filter at the receiver, while [4] and [5] explore adaptation of the linear minimum mean square error (MMSE) receiver and the non-linear MMSE-decision feedback receiver to take into account the ADC presence. Maximum likelihood detection with ADC is investigated in [6], while [7] focuses

on beamforming techniques to improve the performance of a system with low precision ADC.

The special case of 1-bit ADC is particularly interesting, since no AGC is needed. While 1-bit ADC is advantageous in terms of hardware complexity and energy consumption, it generally has a severe impact on performance. Ultra-wideband MIMO systems with 1-bit ADC are studied in [8]. Rayleigh fading MIMO channels with 1-bit ADC are studied in [9]. In [10], an analysis of binary space-time block codes with optimum decoding is provided for systems with 1-bit receive signal quantization. All the above MIMO ADC treatments express the performance in terms of bit-error-rate and/or mutual information.

Massive MIMO as systems, also known as very large MIMO and large-scale antenna systems, have base stations (BSs) equipped with several hundred antennas, which simultaneously serve many tens of terminals in the same time-frequency resource [11]. To be more specific, we define massive MIMO as a system with M BS antennas and K users, where the inequality $M \gg K \gg 1$ holds. Massive MIMO systems are known to be able to average out channel noise and fading [11]–[16]. No investigations have been conducted to decide if massive MIMO systems could be used to average out ADC noise as well. All the contributions on receiver design for massive MIMO systems today assume that the receiver has access to received data with infinite precision.

A. Our contribution

This paper considers the uplink of a massive MIMO system employing 1-bit ADCs. The main difference between our work and the works cited above is that we consider the massive MIMO case, i.e., $M \gg K \gg 1$. Our contributions are the following.

- A discussion of maximum a posteriori probability (MAP) channel estimation with 1-bit ADC is provided. We quantify the computational complexity to be exponential in K . Since this computational complexity is high in a setting with many users, we propose a sub-optimal LS-channel estimation approach.
- We suggest MRC and ZF filters based on the LS channel estimate described under the previous point. We further derive an LS detection filter, which is calculated directly from the uplink training sequences without relying on an intermediate channel estimate.
- We derive an analytical expression for the probability distribution of the MRC filter soft symbol estimates. Using this probability distribution, closed form expressions are developed for both the mutual information between the transmitted symbols and hard symbol estimates and the mutual information between the transmitted symbols and

C. Risi is with the Department of Electrical and Information Engineering (DIEI), University of Cassino and Lazio Meridionale, 03043 Cassino (FR), Italy (E-mail: chiara.risi@unicas.it).

D. Persson and E. G. Larsson are with the Department of Electrical Engineering (ISY), Linköping University, 581 83 Linköping, Sweden (E-mail: danielpl@isy.liu.se, erik.g.larsson@liu.se).

the soft symbol estimates with MRC. The closed-form expression reduces computational complexity in the sense that a Monte Carlo simulation is avoided when computing the mutual information.

- The proposed systems are evaluated by numerical experiments. Both mutual information and SER are investigated. Numerical evaluations of the mutual information and SER are also compared to their closed form expressions. We conclude that massive MIMO provides excellent SER and mutual information performance for wide ranges of system parameters.

The rest of the paper is organized as follows. In Section II, we describe the system model, detection filters, channel estimation methods, and analyze the performance of the system. Our proposed techniques are explored by experiments in Section III. The paper is concluded in Section IV.

Notation: We use boldface lowercase and uppercase letters to denote vectors and matrices respectively.

II. MASSIVE MIMO UPLINK WITH 1-BIT ADC AND NO AGC

This section describes the channel model, suggested solutions, and performance analysis. The system model is detailed in Section II-A, and Section II-B describes the employed detection filters and channel estimation methods. Numerical and analytical procedures for estimating the mutual information are discussed in Section II-C.

A. System model

We consider a single-cell uplink, where there are K single-antenna users and one BS equipped with an array of M antennas. The discrete-time complex baseband received signal at the base station is

$$\mathbf{r} = \sqrt{P_t} \mathbf{H} \mathbf{x} + \mathbf{n}, \quad (1)$$

where $\mathbf{H} \in \mathbb{C}^{M \times K}$ is the channel matrix between the BS and the K users, i.e., h_{ij} is the channel coefficient between the j -th user and the i -th antenna of the BS. The entries of \mathbf{H} are independent $\mathcal{CN}(0, 1)$ random variables. The vector $\mathbf{x} \in \mathbb{C}^K$ contains the transmitted symbols from all the users. In particular, the j -th entry of \mathbf{x} , x_j , is the symbol transmitted by user j . The symbols are modeled as independent identically distributed random variables with zero mean and variance $E[|x_j|^2] = 1$ and, since the spectral efficiency in a massive MIMO system is typically low [17], we assume that they belong to a QPSK constellation. Finally, P_t is the transmit power per user, and $\mathbf{n} \in \mathbb{C}^M$ is the noise vector. The entries of \mathbf{n} are independent identically distributed zero-mean circularly symmetric complex Gaussian random variables, which we denote by $\mathcal{CN}(0, \sigma_N^2)$.

Let $Q(\cdot) : \mathbb{R} \rightarrow \{1, -1\}$ represent the 1-bit ADC quantizer function. It is defined as $Q(u) = \text{sign}(u)$, where $u \in \mathbb{R}$ and $\text{sign}(u)$ is the sign function that returns 1 if $u \geq 0$, and -1 if $u < 0$. For a complex number $v = v_R + jv_I$, $Q(\cdot)$ is applied separately for the real and imaginary parts as $Q(v) =$

$\text{sign}(v_R) + j \text{sign}(v_I)$, and for a vector it is applied element-wise. The quantized received signal is expressed as

$$\mathbf{y} = Q(\mathbf{r}). \quad (2)$$

A soft estimate of the transmitted symbols is obtained by processing the quantized received vector through the receive filter \mathbf{A} as follows

$$\tilde{\mathbf{x}} = \mathbf{A}^H \mathbf{y}. \quad (3)$$

Finally, it is possible to perform a QPSK demodulation that gives as output a hard estimate $\hat{\mathbf{x}}$ of the transmitted vector \mathbf{x} .

B. Receive filters

In order to derive the soft symbol estimates, the receive filter \mathbf{A} needs to be chosen. The channel information needed to compute this filter is acquired through sending uplink pilots. In particular, each coherence time of the channel is divided in two parts. During the first part of it, the users transmit pilot symbols from which the base station calculates the receive filter. During the remainder of the coherence time, all the users transmit their data to the BS, which in turn uses the receive filter calculated from the uplink pilots to detect the symbols. We assume 1-bit analog-to-digital conversion even during the reception of the pilots.

To compute the receive filter \mathbf{A} directly as function of the training sequences, we use a LS approach. The filter obtained via the LS approach is defined as

$$\begin{aligned} \mathbf{A}^H &= \underset{\tilde{\mathbf{A}}}{\text{argmin}} \left(\frac{1}{N} \sum_{n=1}^N \left\| \tilde{\mathbf{A}}^H \mathbf{y}^{(n)} - \mathbf{x}^{(n)} \right\|^2 \right) \\ &= \left(\sum_{n=1}^N \mathbf{x}^{(n)} \left(\mathbf{y}^{(n)} \right)^H \right) \left(\sum_{n=1}^N \mathbf{y}^{(n)} \left(\mathbf{y}^{(n)} \right)^H \right)^{-1}. \end{aligned} \quad (4)$$

In (4), N is the number of time instances used for the pilot transmission, while $\mathbf{x}^{(n)}$ and $\mathbf{y}^{(n)}$ are the transmitted vector and the quantized received vector, respectively, at the n -th time instance dedicated to the training transmission. Note that the matrix $\sum_{n=1}^N \mathbf{y}^{(n)} \left(\mathbf{y}^{(n)} \right)^H$ can be invertible only if $N \geq M$. As a consequence, the LS filter can only be used in a scenario where the channel conditions vary slowly. The LS computational complexity grows linearly with the number of users K and cubically with the number of antennas at the BS M . We have derived the LS receive filter directly from the pilot symbols. Another possibility is to derive an estimate of the channel matrix \mathbf{H} first, and then calculate the filter based on the channel state information (CSI).

For MAP-optimal channel estimation, we calculate

$$\hat{\mathbf{H}} = \underset{\mathbf{H}}{\text{argmax}} p(\mathbf{H}|\mathbf{Y}) = \underset{\mathbf{H}}{\text{argmax}} p(\mathbf{Y}|\mathbf{H})p(\mathbf{H}), \quad (5)$$

where $\mathbf{Y} = [\mathbf{y}^{(1)}, \dots, \mathbf{y}^{(N)}]$, $\mathbf{X} = [\mathbf{x}^{(1)}, \dots, \mathbf{x}^{(N)}]$, $p(\mathbf{H}|\mathbf{Y})$ is the probability density function (pdf) of \mathbf{H} given \mathbf{Y} , $p(\mathbf{Y}|\mathbf{H})$ is the probability mass function (pmf) of \mathbf{Y} given \mathbf{H} , and $p(\mathbf{H})$ is the pdf of \mathbf{H} . By independence of the variables involved at different antennas, the optimization problem in (5) is equivalent to

$$\hat{\mathbf{h}}_i = \underset{\mathbf{h}_i}{\text{argmax}} p(\mathbf{Y}_i|\mathbf{h}_i) p(\mathbf{h}_i), \quad i = 1, \dots, M, \quad (6)$$

where $\hat{\mathbf{h}}_i^T$, \mathbf{h}_i^T , and \mathbf{Y}_i^T are the i -th rows of $\hat{\mathbf{H}}$, \mathbf{H} , and \mathbf{Y} respectively, $p(\mathbf{Y}_i|\mathbf{h}_i)$ is the pmf of \mathbf{Y}_i given \mathbf{h}_i , and $p(\mathbf{h}_i)$ is the pdf of \mathbf{h}_i . In order to solve the i -th optimization problem in (6), we have to resort to a grid search method. In particular, the space \mathbb{C} is discretized so that h_{ij} belongs to a finite set $\mathcal{A} \forall i, j$. The BS has to search over all possible vectors \mathbf{h}_i , and there are $|\mathcal{A}|^K$ such vectors. Therefore, MAP estimation has a computational complexity that is exponential in the number of users. A main benefit of massive MIMO is to be able to multiplex many users, i.e., $K \gg 1$, and we can conclude that MAP channel estimation is less suitable for this application.

To reduce the computational complexity, we use the LS estimator. The LS estimate of \mathbf{H} is given by

$$\begin{aligned} \hat{\mathbf{H}} &= \underset{\hat{\mathbf{H}}}{\operatorname{argmin}} \sum_{n=1}^N \left\| \mathbf{y}^{(n)} - \sqrt{P_t} \hat{\mathbf{H}} \mathbf{x}^{(n)} \right\|^2 \\ &= \left(\sum_{n=1}^N \sqrt{P_t} \mathbf{y}^{(n)} \mathbf{x}^{(n)H} \right) \left(\sum_{n=1}^N P_t \mathbf{x}^{(n)} \mathbf{x}^{(n)H} \right)^{-1}. \end{aligned} \quad (7)$$

Note that, in this case, we need at least K training symbol transmissions for the matrix $\sum_{n=1}^N \mathbf{x}^{(n)} \mathbf{x}^{(n)H}$ to be invertible. The computational complexity, instead, grows linearly with the number of antennas at the BS M and cubically with the number of users K . The computational complexity reduction with respect to (4) is thus significant. Lastly, we refer to $\hat{\mathbf{H}} = \mathbf{H}$ as the case of full CSI.

The next step is to derive the receive filter \mathbf{A} based on the LS $\hat{\mathbf{H}}$ -estimate. We consider two conventional linear detectors, namely the MRC and the ZF. The MRC is defined as

$$\mathbf{a}^i = \frac{\hat{\mathbf{h}}^i}{\|\hat{\mathbf{h}}^i\|^2}, \quad (8)$$

where \mathbf{a}^i and $\hat{\mathbf{h}}^i$ are the i -th columns of \mathbf{A} and $\hat{\mathbf{H}}$, respectively. The ZF is defined as

$$\mathbf{A}^H = \hat{\mathbf{H}}^\dagger, \quad (9)$$

where $\hat{\mathbf{H}}^\dagger = \left(\hat{\mathbf{H}}^H \hat{\mathbf{H}} \right)^{-1} \hat{\mathbf{H}}^H$ is the pseudoinverse of the matrix $\hat{\mathbf{H}}$.

C. Performance metrics

In this section, we consider two performance metrics: the mutual information per user and the SER per user. We show how they can be calculated numerically and analytically.

1) *Mutual information*: The average mutual information of the discrete channel between the transmitted QPSK symbol x_k and the QPSK symbol estimate \hat{x}_k is defined as

$$I(x_k; \hat{x}_k) = \mathbb{E}_{\mathbf{H}} \left[\sum_{x_k, \hat{x}_k} p(\hat{x}_k|x_k, \mathbf{H}) p(x_k) \log_2 \frac{p(\hat{x}_k|x_k, \mathbf{H})}{p(\hat{x}_k|\mathbf{H})} \right], \quad (10)$$

where $p(\hat{x}_k|x_k, \mathbf{H})$ is the pmf of \hat{x}_k given x_k and \mathbf{H} , $p(x_k)$ is the pmf of a QPSK constellation with uniformly distributed symbols, and $p(\hat{x}_k|\mathbf{H}) = \sum_{x_k} p(\hat{x}_k|x_k, \mathbf{H}) p(x_k)$.

In a case where the mutual information is evaluated numerically, $p(\hat{x}_k|x_k, \mathbf{H})$ is estimated through Monte Carlo simulations with many realizations of the transmit vector \mathbf{x} and the channel noise vector \mathbf{n} . In what follows, we give an alternative to the Monte Carlo evaluation of $p(\hat{x}_k|x_k, \mathbf{H})$.

To calculate the transition probabilities $p(\hat{x}_k|x_k, \mathbf{H})$, we need to find first $f(\hat{x}_k|x_k, \mathbf{H})$, which is the pdf of \hat{x}_k given x_k and \mathbf{H} . Considering a matched filtering, note that \tilde{x}_k can be rewritten as

$$\begin{aligned} \tilde{x}_k &= \sum_{i=1}^M \frac{h_{ik}^*}{\|\mathbf{h}_k\|^2} y_i \\ &= \sum_{i=1}^M \left(\frac{h_{ik}^*}{\|\mathbf{h}_k\|^2} y_i - \mu_i + \mu_i \right) \\ &= \sum_{i=1}^M \left(\frac{h_{ik}^*}{\|\mathbf{h}_k\|^2} y_i - \mu_i \right) + \sum_{i=1}^M \mu_i, \end{aligned} \quad (11)$$

where $\mu_i = \mathbb{E}_{y_i} \left[\frac{h_{ik}^*}{\|\mathbf{h}_k\|^2} y_i | x_k, \mathbf{H} \right] = \frac{h_{ik}^*}{\|\mathbf{h}_k\|^2} \sum_{c=1}^4 p_{ic} s_c$, $p_{ic} = \operatorname{Prob}(y_i = s_c | x_k, \mathbf{H})$ and $s_1 = 1+j$, $s_2 = 1-j$, $s_3 = -1-j$, $s_4 = -1+j$.

In order to calculate $p(\hat{x}_k|x_k, \mathbf{H})$, we use the Cramer's central limit theorem [18], [19], which states that the sum $\sum_{i=1}^L u_i$ of a large number of independent random variables is approximately complex Gaussian if the following conditions are satisfied:

- 1) every component u_i has a zero mean value,
- 2) every component u_i has a finite variance $a_i^2 = \mathbb{E}[|u_i|^2]$,
- 3) $\frac{a_i}{s_L} \xrightarrow{L \rightarrow \infty} 0$ and $s_L \xrightarrow{L \rightarrow \infty} \infty$, where $s_L = \sum_{i=1}^L a_i^2$.

To apply the Cramer's central limit theorem to (11), we define $z_i = \left[\left(\frac{h_{ik}^*}{\|\mathbf{h}_k\|^2} y_i - \mu_i \right) | x_k, \mathbf{H} \right]$, and we make Assumption (A) that z_i and z_j are independent for all i, j such that $i \neq j$. Further in this section, we will show that, with Assumption (A), the approximated pdf of \tilde{x}_k derived below fits well with the real probability distribution, and in Section III, we will show that the performance evaluation based on the approximated pdf closely match the Monte Carlo symbol and noise vectors simulation results.

Applying the Cramer's central limit theorem with (11) and Assumption (A) above, we have that

$$\tilde{x}_k | x_k, \mathbf{H} \xrightarrow{M \rightarrow \infty} \mathcal{CN} \left(\sum_{i=1}^M \mu_i, \sum_{i=1}^M \sigma_i^2 \right), \quad (12)$$

where $\sigma_i^2 = \frac{|h_{ik}|^2}{\|\mathbf{h}_k\|^4} \left(2 - |\sum_{c=1}^4 p_{ic} s_c|^2 \right)$. In order to calculate p_{ic} , we consider

$$y_i = \operatorname{sign} \left(\overbrace{\sqrt{P_t} h_{ik} x_k + \sqrt{P_t} \sum_{j=1, j \neq k}^K h_{ij} x_j + n_i}^{T_i} \right). \quad (13)$$

Rewriting I as

$$\begin{aligned} I &= \sqrt{P_t} \sum_{j=1, j \neq k}^K h_{ij} x_j \\ &= \sqrt{P_t} \sum_{j=1, j \neq k}^K (h_{ij} x_j - \mu_j^I) + \sqrt{P_t} \sum_{j=1, j \neq k}^K \mu_j^I, \end{aligned} \quad (14)$$

with $\mu_j^I = \mathbb{E}_{x_j} [h_{ij} x_j | h_{ij}] = 0$, we can again apply the Cramer central limit theorem on $\sum_{j=1, j \neq k}^K (h_{ij} x_j - \mu_j^I)$ and find that

$$r_i | x_k, \mathbf{H} \xrightarrow{K \rightarrow \infty} \mathcal{CN} \left(\sqrt{P_t} h_{ik} x_k, P_t \underbrace{\sum_{j=1, j \neq k}^K |h_{ij}|^2}_{(\sigma^I)^2} + \sigma_N^2 \right). \quad (15)$$

The superscript $(\cdot)^I$ of the parameters μ_j^I and $(\sigma^I)^2$ is used to indicate that they are related to the interference term in (14). Noticing that the real and imaginary parts of r_i given x_k and \mathbf{H} are independent, and that they have the same variance, the probabilities p_{ic} can be calculated using complementary error functions. In particular, for $x_k = \frac{1}{\sqrt{2}} + j \frac{1}{\sqrt{2}}$ they are derived as follows

$$\begin{aligned} p_{i1} &= \text{Prob} \left(y_i = 1 + j | x_k = \frac{1}{\sqrt{2}} + j \frac{1}{\sqrt{2}}, \mathbf{H} \right) \\ &= \frac{1}{2} \text{erfc} \left(-\frac{\sqrt{P_t} \text{Re}(h_{ik} x_k)}{\sqrt{\sigma_N^2 + (\sigma^I)^2}} \right) \\ &\quad \cdot \frac{1}{2} \text{erfc} \left(-\frac{\sqrt{P_t} \text{Im}(h_{ik} x_k)}{\sqrt{\sigma_N^2 + (\sigma^I)^2}} \right), \end{aligned} \quad (16)$$

$$\begin{aligned} p_{i2} &= \text{Prob} \left(y_i = 1 - j | x_k = \frac{1}{\sqrt{2}} + j \frac{1}{\sqrt{2}}, \mathbf{H} \right) \\ &= \frac{1}{2} \text{erfc} \left(-\frac{\sqrt{P_t} \text{Re}(h_{ik} x_k)}{\sqrt{\sigma_N^2 + (\sigma^I)^2}} \right) \\ &\quad \cdot \left(1 - \frac{1}{2} \text{erfc} \left(-\frac{\sqrt{P_t} \text{Im}(h_{ik} x_k)}{\sqrt{\sigma_N^2 + (\sigma^I)^2}} \right) \right), \end{aligned} \quad (17)$$

$$\begin{aligned} p_{i3} &= \text{Prob} \left(y_i = -1 - j | x_k = \frac{1}{\sqrt{2}} + j \frac{1}{\sqrt{2}}, \mathbf{H} \right) \\ &= \left(1 - \frac{1}{2} \text{erfc} \left(-\frac{\sqrt{P_t} \text{Re}(h_{ik} x_k)}{\sqrt{\sigma_N^2 + (\sigma^I)^2}} \right) \right) \\ &\quad \cdot \left(1 - \frac{1}{2} \text{erfc} \left(-\frac{\sqrt{P_t} \text{Im}(h_{ik} x_k)}{\sqrt{\sigma_N^2 + (\sigma^I)^2}} \right) \right), \end{aligned} \quad (18)$$

$$\begin{aligned} p_{i4} &= \text{Prob} \left(y_i = 1 - j | x_k = \frac{1}{\sqrt{2}} + j \frac{1}{\sqrt{2}}, \mathbf{H} \right) \\ &= \left(1 - \frac{1}{2} \text{erfc} \left(-\frac{\sqrt{P_t} \text{Re}(h_{ik} x_k)}{\sqrt{\sigma_N^2 + (\sigma^I)^2}} \right) \right) \\ &\quad \cdot \frac{1}{2} \text{erfc} \left(-\frac{\sqrt{P_t} \text{Im}(h_{ik} x_k)}{\sqrt{\sigma_N^2 + (\sigma^I)^2}} \right), \end{aligned} \quad (19)$$

and similarly for other possible values of x_k . Knowing how to calculate p_{ic} as in (16) to (19), (12) now gives us the distribution of \tilde{x}_k given x_k and \mathbf{H} .

In order to validate the model (12) derived using Assumption (A) for the soft symbol estimate, we provide the results in Figure 1. The plot is divided in a 3×2 grid. The conditional probability distribution function of the real part of \tilde{x}_k given x_k and \mathbf{H} is depicted in the first column, while the distribution of the imaginary part of \tilde{x}_k given x_k and \mathbf{H} is depicted in the second column. The distributions are calculated both by Monte Carlo simulation and analytically, as in (12). Further, each row corresponds to a different random channel realization. We consider a 400-antenna BS that serves $K = 20$ users. The symbol x_k transmitted by user k is $\frac{1}{\sqrt{2}} + j \frac{1}{\sqrt{2}}$. The signal-to-noise ratio (SNR) is set to -20 dB, where the SNR is defined as P_t / σ_N^2 . The results remain similar for all other SNR values, and for all tested matrix realizations. From Figure 1, we observe that the derived pdf in (12) closely matches the distribution obtained by Monte Carlo simulation.

Once that $f(\tilde{x}_k | x_k, \mathbf{H})$ is known, the transition probabilities $p(\tilde{x}_k | x_k, \mathbf{H})$ can be calculated either numerically or using complementary error functions. Finally, the mutual information associated with the discrete channel between x_k and \tilde{x}_k is calculated as in (10).

In what follows, we also introduce the mutual information between the transmitted QPSK symbol x_k and the soft symbol estimate \tilde{x}_k . It is defined as

$$\begin{aligned} I(x_k; \tilde{x}_k) &= \\ &= \int \mathbb{E}_{\mathbf{H}} \left[\sum_{x_k} f(\tilde{x}_k | x_k, \mathbf{H}) p(x_k) \log_2 \frac{f(\tilde{x}_k | x_k, \mathbf{H})}{f(\tilde{x}_k | \mathbf{H})} \right] d\tilde{x}_k. \end{aligned} \quad (20)$$

The integral over \tilde{x}_k is calculated by discretization of the continuous random variable \tilde{x}_k . The resulting discrete random variable is \tilde{x}_k^Δ , and the mutual information between \tilde{x}_k^Δ and x_k is given by

$$\begin{aligned} I(x_k; \tilde{x}_k^\Delta) &= \\ &= \mathbb{E}_{\mathbf{H}} \left[\sum_{x_k, \tilde{x}_k^\Delta} p(\tilde{x}_k^\Delta | x_k, \mathbf{H}) p(x_k) \log_2 \frac{p(\tilde{x}_k^\Delta | x_k, \mathbf{H})}{p(\tilde{x}_k^\Delta | \mathbf{H})} \right], \end{aligned} \quad (21)$$

where $p(\tilde{x}_k^\Delta | x_k, \mathbf{H})$ is the pmf of \tilde{x}_k^Δ given x_k and \mathbf{H} , and $p(\tilde{x}_k^\Delta | \mathbf{H}) = \sum_{x_k} p(\tilde{x}_k^\Delta | x_k, \mathbf{H}) p(x_k)$. Note again that $p(\tilde{x}_k^\Delta | x_k, \mathbf{H})$ does not need to be estimated by Monte Carlo simulations based on many realizations of the transmit vector \mathbf{x} and the channel noise vector \mathbf{n} . Instead we can rely on (12).

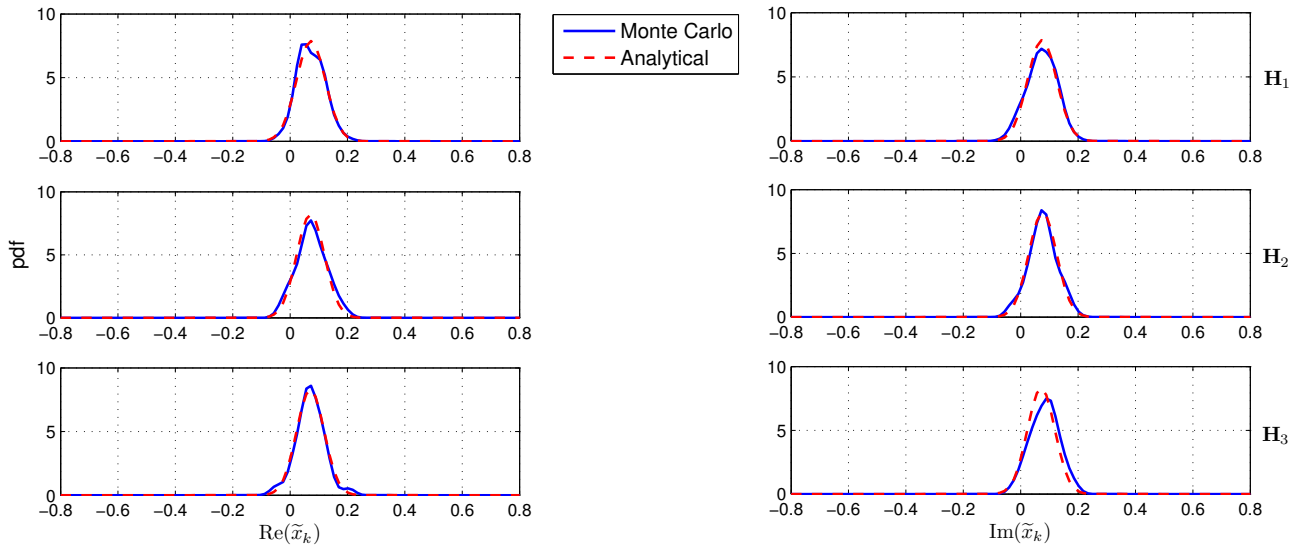


Fig. 1. Probability distribution of the real and imaginary parts of \tilde{x}_k given $x_k = \frac{1}{\sqrt{2}} + j\frac{1}{\sqrt{2}}$ and \mathbf{H} , considering $M = 400$ and $K = 20$. Three different channel matrices are considered, and the SNR is set to -20 dB.

2) *SER*: The average SER of user k is expressed as

$$\text{SER} = p(\hat{x}_k \neq x_k) \quad (22)$$

$$= E_{\mathbf{H}} \left[\sum_{x_k} \sum_{\hat{x}_k \neq x_k} p(\hat{x}_k | x_k, \mathbf{H}) p(x_k) \right], \quad (23)$$

where $p(\hat{x}_k \neq x_k)$ is the probability that the QPSK symbol estimate \hat{x}_k is different from the transmitted QPSK symbol x_k .

In a case where the SER is evaluated numerically, $p(\hat{x}_k \neq x_k)$ in (22) is estimated through Monte Carlo simulations with many realizations of the transmit vector \mathbf{x} , the channel noise vector \mathbf{n} , and the channel matrix \mathbf{H} .

When the MRC filter is employed, we can alternatively use (23) to calculate the SER. The transition probabilities $p(\hat{x}_k | x_k, \mathbf{H})$ in (23) are calculated as described in the previous section for the analytical evaluation of the mutual information.

III. SIMULATION RESULTS

We will compare the proposed schemes in terms of Monte Carlo channel simulations. If nothing else is mentioned, the results have been obtained numerically by Monte Carlo simulations, i.e., not by the analytical treatment employing (12). Moreover, if nothing else is mentioned, the mutual information based on (10) associated with the discrete channel between the transmitted and received QPSK symbols x_k and \hat{x}_k is depicted, i.e., the mutual information per user between the transmitted QPSK symbol x_k and the soft symbol estimate \tilde{x}_k defined as in (21) is not depicted.

Symbol and noise vectors Monte Carlo simulation mutual information is obtained by averaging the mutual information over 10^2 channel matrix realizations, and for each channel realization, 10^2 random symbol and noise vectors realizations are used. Symbol and noise vectors Monte Carlo simulation

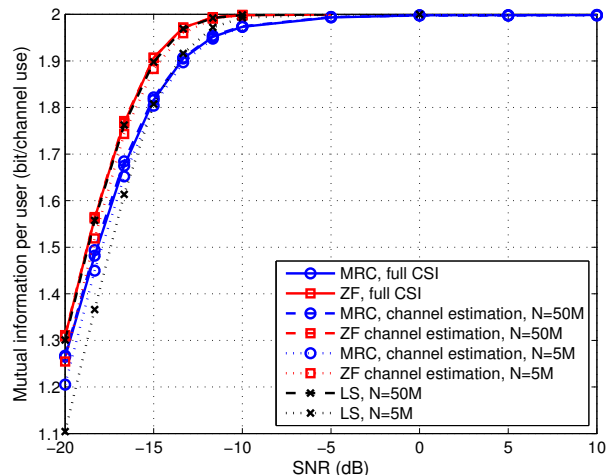


Fig. 2. Mutual information per user based on (10) versus SNR for $M = 400$ and $K = 20$, and MRC, ZF, and LS filters. The MRC and ZF are considered for both the cases of perfect and imperfect CSI.

SER graphs, instead, are obtained by averaging over 10^5 channel matrix, symbol and noise vectors realization triplets. Analytic analysis curves based on (12) are obtained by averaging the mutual information over 10^2 independent random channel matrix realizations and the SER over 10^5 channel random channel matrix realizations.

Figure 2 shows the mutual information per user versus the SNR for MRC, ZF, and LS receivers, with $M = 400$ antennas at the BS that serve $K = 20$ users. The MRC and the ZF filters are investigated for both the cases of full CSI and imperfect channel knowledge. In order to calculate the channel estimate in (7) and the LS filter matrix in (4), we choose pilot sequences of length $N = 5M$ and $N = 50M$. The pilot sequences are randomly generated. It is seen that the LS filter requires around

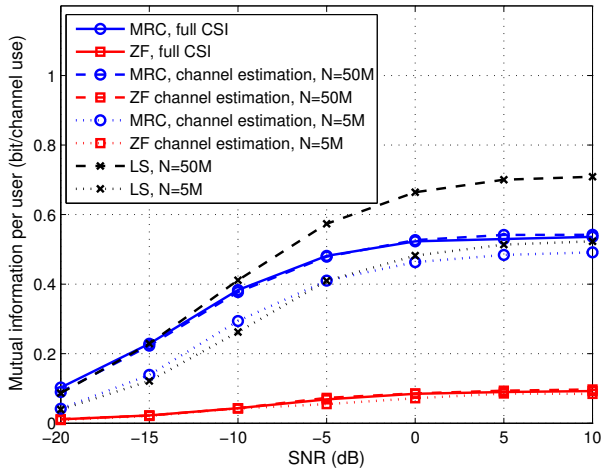


Fig. 3. Mutual information per user based on (10) versus SNR for $M = 20$ and $K = 20$, and MRC, ZF, and LS filters. The MRC and ZF are considered for both the cases of perfect and imperfect CSI.

$N = 50M$ time slots to achieve the same performance as the full CSI ZF filter. The MRC and ZF filters, instead, exhibit a faster convergence, so that they require shorter training phase (the channel estimation error is almost suppressed using $N = 5M$ time slots), as explained in Section II-B.

Figure 3 is organized in the same way, but considering a BS equipped with $M = 20$ antennas and $K = 20$ users. Differently from the massive MIMO case, here the LS filter is performing better with respect to the ZF and MRC when $N = 50M$. However, the performance of all methods is lower compared to that achieved by a massive MIMO system. Since the LS filter needs more training data to perform well in the massive MIMO case, as is seen in Figure 2, and since it also needs higher computational complexity compared to the ZF and MRC channel estimation, as discussed in Section II-B, we do not consider it in the following.

Focusing the attention on the MRC and the ZF receivers, in Figure 4 and Figure 5 the mutual information per user versus the SNR and the SER per user versus the SNR are depicted, respectively. The aim of the graphs is to show how the length of the training sequences N affects the performance. In particular, we consider three values of N : $5K$, $10K$, and $50K$. As we can see from the figures, to achieve the same performance as the full CSI case we have to use a long training sequence. This is possible in a scenario where the environment does not vary very fast. However, for values of SNR greater than -5 dB, the MRC and the ZF filters are equivalent in terms of mutual information, and the channel estimation error is suppressed even for short training sequences. In this same SNR regime, the maximal possible QPSK capacity of 2 bits is obtained.

In Figure 6 and Figure 7, we show the performance gap between the case in which the quantizer is considered in the system model and the case in which it is not considered. We show the mutual information per user versus the SNR and the SER per user versus the SNR, respectively, for the ZF receiver. Both the cases of full CSI and imperfect CSI are depicted. For

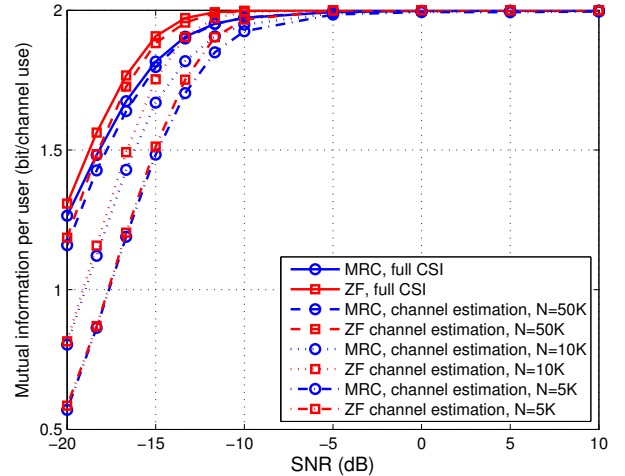


Fig. 4. Mutual information per user based on (10) versus SNR for $M = 400$ and $K = 20$. The ZF and MRC filters are considered for both the cases of perfect and imperfect CSI.

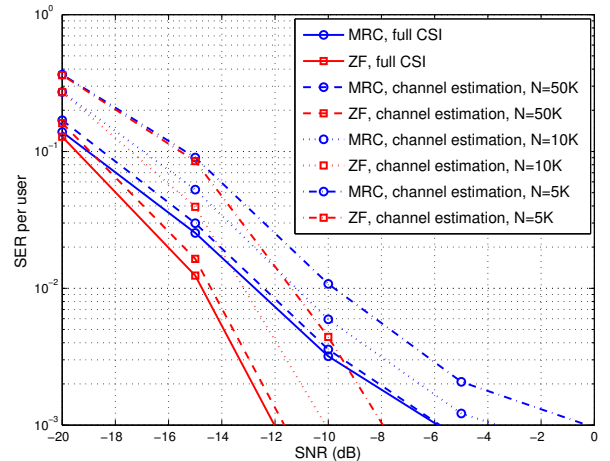


Fig. 5. SER per user versus SNR for $M = 400$ and $K = 20$. The ZF and MRC filters are considered for both the cases of perfect and imperfect CSI.

the channel estimation phase, a training sequence of length $N = 50K$ has been used. From the figures, we observe that the scenario in which the channel is assumed to be perfectly known at the receiver and the quantizer effects are neglected gives an upper bound on the performance. We also note that, for values of SNR larger than -10 dB, the mutual information achieves the maximum possible QPSK mutual information of 2 bits in all the four considered cases.

All the above results have been obtained numerically by symbol and noise vectors Monte Carlo simulations. In order to verify the analytical analysis in Section II, Figure 8 and Figure 9 compare the performance obtained using (12) with those obtained by Monte Carlo symbol and noise vectors simulations. In particular, Figure 8 depicts the mutual information per user versus the SNR, while Figure 9 shows the SER per user versus the SNR. For the analytical curves, the transition probabilities $p(\hat{x}_k|x_k)$ are calculated using complementary error functions

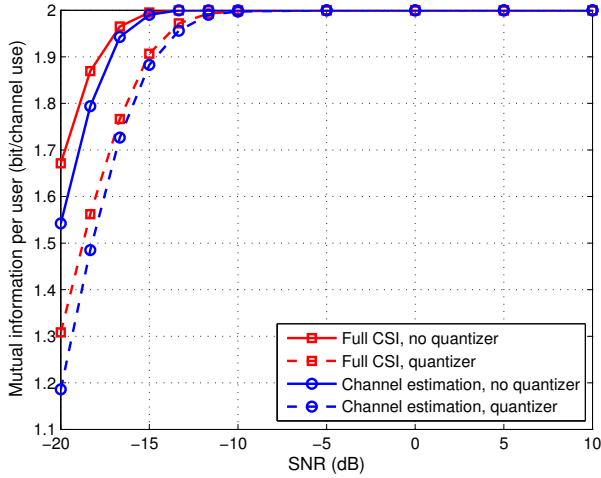


Fig. 6. Mutual information per user based on (10) versus SNR considering $M = 400$ and $K = 20$, for the case in which the quantizer is taken into account and the case in which it is not. The ZF is considered for both the cases of perfect and imperfect CSI.

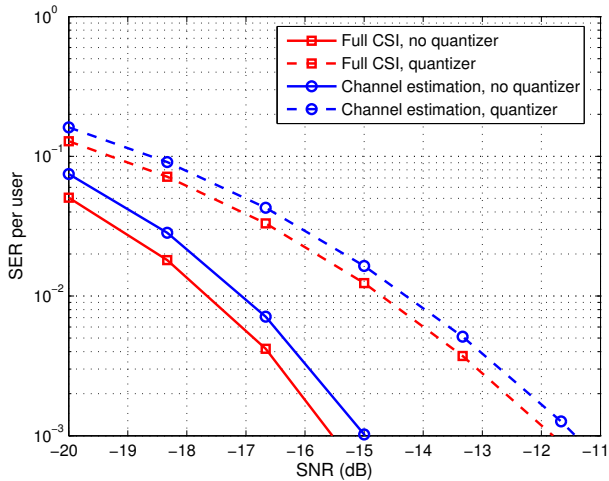


Fig. 7. SER per user versus SNR considering $M = 400$ and $K = 20$, for the case in which the quantizer is taken into account and the case in which it is not. The ZF is considered for both the cases of perfect and imperfect CSI.

and (12). The mutual information based on (10) associated with the discrete channel between the transmitted and received QPSK symbols x_k and \hat{x}_k , as well as the mutual information per user between the transmitted QPSK symbol x_k and the soft symbol estimate \tilde{x}_k defined as in (21), are depicted in Figure 8. In Figure 9, the analytical results are based on the SER expression defined in (23).

The graphs show that the results based on the analytical treatment closely match the symbol and noise vectors Monte Carlo simulation results. As expected in Figure 8, the mutual information soft symbol estimate (21) is larger than the mutual information in (10) associated with the discrete channel.

IV. CONCLUSIONS

This paper has examined the performance of a massive MIMO uplink system that employs 1-bit ADCs. Numerical

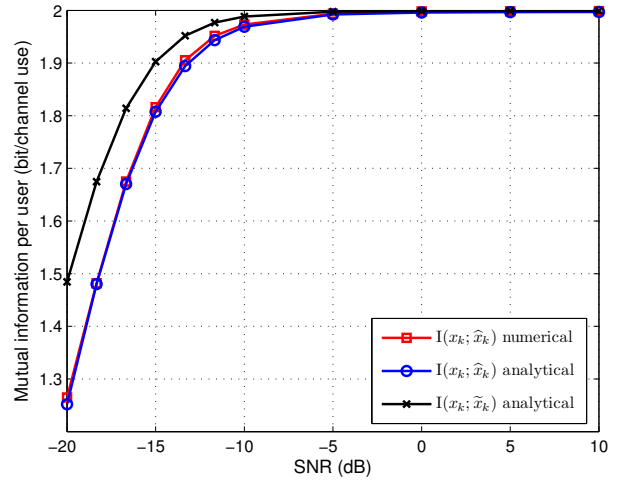


Fig. 8. Mutual information per user versus SNR considering $M = 400$ and $K = 20$, and the MRC filter with full CSI. Monte Carlo symbol and noise vectors simulation results are compared with the analytical results based on (12). The mutual information based on (10) associated with the discrete channel between the transmitted and received QPSK symbols x_k and \hat{x}_k , as well as the mutual information per user between the transmitted QPSK symbol x_k and the soft symbol estimate \tilde{x}_k defined as in (21), are depicted.

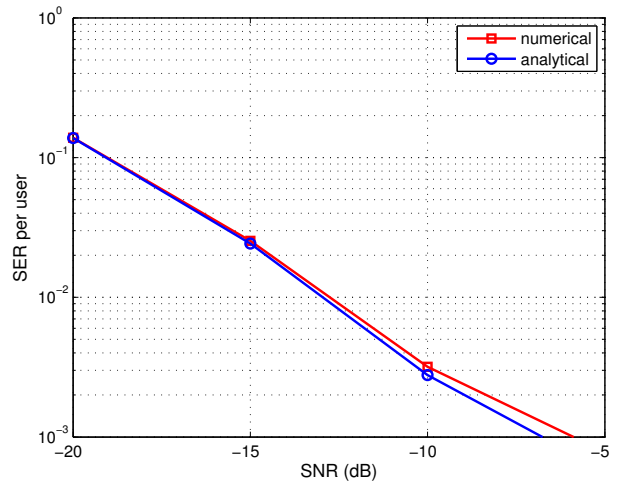


Fig. 9. SER per user versus SNR considering $M = 400$ and $K = 20$, and the MRC filter with full CSI. Monte Carlo symbol and noise vectors simulation results are compared with the analytical results based on (12) and (23).

evaluation of the mutual information and the symbol error rate have been provided for MRC, ZF, and LS receive filters. While the LS filter has been directly calculated depending on the uplink training sequences, the MRC and ZF filters have been derived based on the CSI estimate. We provided a discussion of MAP channel estimation but, due to the high computational complexity in a setting with many users, we suggested a sub-optimal LS-channel estimation approach. We have also shown how the training sequence length affects the performance, and the performance gap between the scenario with a quantized receive vector and the scenario with an unquantized receive vector. In general, the ZF filter shows

better performance compared to the MRC and the LS filters. However, when the SNR is larger than a certain value, all the filters achieve the maximal possible QPSK capacity, whatever the training sequence length is, and for both the quantized and the unquantized cases.

Further, an analytical analysis of the performance is provided for the MRC filters. We showed that the results based on the analytical analysis fit well to the Monte Carlo results. Thanks to the closed-form derivation of the symbol estimate pmf, the computational complexity is reduced in the sense that a symbol and channel noise vectors Monte Carlo simulation is avoided. Concluding, we have showed that massive MIMO systems exhibit good performance even when employing 1-bit receive signal quantization. Thus, the ADC implementation complexity and power consumption can be eliminated.

REFERENCES

- [1] E. Dahlman, S. Parkvall, J. Skold, and P. Beming, *3G evolution: HSPA and LTE for mobile broadband*. Access Online via Elsevier, 2010.
- [2] R. Schreier, G. C. Temes, and J. Wiley, *Understanding delta-sigma data converters*. IEEE press Piscataway, NJ, 2005.
- [3] B. Murray and I. Collings, "AGC and quantization effects in a zero-forcing MIMO wireless system," in *IEEE Vehicular Technology Conference*, 2006.
- [4] A. Mezghani, M.-S. Khoufi, and J. A. Nossek, "A modified MMSE receiver for quantized MIMO systems," *ITG/IEEE Workshop on Smart Antennas*, 2007.
- [5] A. Mezghani, M.-S. Khoufi, and J. Nossek, "Spatial MIMO decision feedback equalizer operating on quantized data," in *IEEE International Conference on Acoustics, Speech and Signal Processing*, 2008.
- [6] —, "Maximum likelihood detection for quantized MIMO systems," in *Smart Antennas, 2008. WSA 2008. International ITG Workshop on*, Feb 2008, pp. 278–284.
- [7] T. Shah and O. Dabeer, "Transmit beamforming for MIMO communication systems with low precision adc at the receiver," *CoRR*, vol. abs/1310.1571, 2013.
- [8] A. Mezghani and J. Nossek, "On ultra-wideband MIMO systems with 1-bit quantized outputs: Performance analysis and input optimization," in *IEEE International Symposium on Information Theory*, 2007.
- [9] —, "Analysis of rayleigh-fading channels with 1-bit quantized output," in *IEEE International Symposium on Information Theory*, 2008.
- [10] M. Ivrlac and J. Nossek, "Challenges in coding for quantized MIMO systems," in *IEEE International Symposium on Information Theory*, 2006.
- [11] F. Rusek, D. Persson, B. K. Lau, E. Larsson, T. Marzetta, O. Edfors, and F. Tufvesson, "Scaling up MIMO: Opportunities and challenges with very large arrays," *IEEE Signal Processing Magazine*, vol. 30, no. 1, pp. 40–60, 2013.
- [12] E. Larsson, O. Edfors, F. Tufvesson, and T. Marzetta, "Massive MIMO for next generation wireless systems," *IEEE Communications Magazine*, vol. 52, no. 2, pp. 186–195, 2014.
- [13] J. Hoydis, K. Hosseini, S. ten Brink, and M. Debbah, "Making smart use of excess antennas: Massive MIMO, small cells, and TDD," *Bell Labs Technical Journal*, vol. 18, no. 2, pp. 5–21, 2013.
- [14] T. Marzetta, "Noncooperative cellular wireless with unlimited numbers of base station antennas," *IEEE Transactions on Wireless Communications*, vol. 9, no. 11, pp. 3590–3600, 2010.
- [15] J. Hoydis, S. ten Brink, and M. Debbah, "Massive MIMO: How many antennas do we need?" in *IEEE Annual Allerton Conference on Communication, Control, and Computing*, 2011.
- [16] H. Q. Ngo, E. Larsson, and T. Marzetta, "Energy and spectral efficiency of very large multiuser MIMO systems," *IEEE Transactions on Communications*, vol. 61, no. 4, pp. 1436–1449, 2013.
- [17] H. Yang and T. Marzetta, "Total energy efficiency of cellular large scale antenna system multiple access mobile networks," in *IEEE Online Conference on Green Communications*, 2013.
- [18] H. Cramér, *Random variables and probability distributions*. Cambridge University Press, 2004.
- [19] A. Shah and A. Haimovich, "Performance analysis of maximal ratio combining and comparison with optimum combining for mobile radio communications with cochannel interference," *IEEE Transactions on Vehicular Technology*, vol. 49, no. 4, pp. 1454–1463, 2000.